IEEE Access
Multidisciplinary | Rapid Review | Open Access Journal

Received June 25, 2017, accepted July 13, 2017, date of publication July 20, 2017, date of current version August 22, 2017.

Digital Object Identifier 10.1109/ACCESS.2017.2729517

Multimode and Wideband Printed Loop Antenna Based on Degraded Split-Ring Resonators

KUIWEN XU[1], FEI LIU[1], LIANG PENG[1], WEN-SHENG ZHAO[1], (Member, IEEE), LIXIN RAN[2], AND GAOFENG WANG[1], (Senior Member, IEEE)

[1]Key Lab of RF Circuits and Systems of Ministry of Education, Hangzhou Dianzi University, Hangzhou 310018, China
[2]Laboratory of Applied Research on Electromagnetics, Zhejiang University, Hangzhou 310027, China

Corresponding author: Gaofeng Wang (gaofeng@hdu.edu.cn)

This work was supported by the NSFC under Grant 61601161, Grant 61411136003, and Grant 61331007.

ABSTRACT In this paper, a compound multimode printed loop antenna based on degraded spilt-ring resonators (SRRs) for broadband wireless applications is proposed. The proposed antenna consists of an outer split ring and one inner closed ring with a big difference in size, which can be considered as degraded SRRs. By virtue of the orthogonal radiating mode of two rings, the compound multimode loop antenna can achieve multi-band resonances. Collaborating with the two coupled rings, a parasitic strip is placed close to the feed gap of the inner ring, which not only induces a new resonant frequency at upper band but also greatly improves the impedance matching in all high-frequency bands. The proposed antenna not only covers the first split ring mode at 816 MHz but also exhibits a broadband property covering from 2.3 to 4.6 GHz (reflection coefficient $|S_{11}| < -10$ dB, 67% fractional bandwidth). The antenna operational principle and physical mechanism are analyzed by carrying out the studies of mode analysis and surface current distribution. To demonstrate the effectiveness of the proposed antenna, an antenna prototype is fabricated and tested. It is numerically and experimentally proved that broadband and multimode characteristics, stable radiation patterns with a peak gain of 1.2 and 5.1 dBi in the low- and high-frequency bands respectively, and more than 80% efficiency can be achieved. With merits of a compact size of $0.12\lambda_0 \times 0.11\lambda_0$ (λ_0 is the wavelength at the lowest operating frequency), uniplanar and simple printed structure and wide bandwidth characteristics make it suitable for a wide range of wireless applications.

INDEX TERMS Radiating mode and non-radiating mode, split-ring resonators (SRRs), closed ring, dipole antenna, loop antenna, magnetic and electric couplings, wideband antenna.

I. INTRODUCTION

Nowadays, with rapid development of wireless communication systems, antennas with low cost, low profile, compact size, wide impedance bandwidth and unidirectional radiation are increasingly demanded for a wide variety of applications, such as point to point communication, RFID systems, microwave imaging, internet of things [1]–[4]. Although achieving one of aforementioned requirements seems to be facile, designing a single antenna satisfying some or all of them is a challenging task.

Various antenna design techniques have been developed to achieve the goals above [5]–[9]. Among them, printed antennas are good candidate in small device applications owing to their merits such as miniature size, easy-integration and fabrication, omnidirectional-like radiation, etc. In order to minimize the structure size, improve impedance matching and achieve wideband characteristics, there are various designs of printed antennas reported in previously published literature, such as dipole antennas, CPW-fed monopole antenna, log-periodic antenna, Yagi-like antenna and so on [10]–[14]. In all these antennas, the ultra-band characteristics of printed antennas are realized mainly by dipole/monopole-like composite radiators with various structures. However, since the sizes of these antennas are primarily determined by the longest electrical lengths of the surface currents at the lowest frequency, some of these designs are too large in geometrical size and not suitable for small wireless device implementation. Within limited area, it is also very difficult to cover the frequencies below 3 GHz, particularly below 1 GHz.

From the electromagnetic theory, magnetic and electric dipole antennas are mutually dual. Owing to simple printed structure and the easy integration with other components

of conventional loop antenna, it is widely used in various wireless applications. However, classic loop antennas are typical narrow band radiators and occupy much space. Recently some wideband antennas with loop or loop-dipole composite structures have been widely reported in [15]–[20]. A design of rectangular loop with two capacitive gaps has been proposed in [15], which can attain a unidirectional radiation with good front-to-back ratio (more than 20 dB). In order to improve bandwidth and band-edge selectivity, a unidirectional loop with an addition parametric loop was presented in [16]. Based on rectangular slot-loaded loop antenna, exploratory studies have been performed to achieve wideband performance and stable radiation characteristics [17]–[19]. In all these loop antennas above, direct feeding technique on the loop has been adopted. In addition, there have been a large number of designs by way of exciting magnetic dipole and electric dipole (ME dipole/ loop-dipole) simultaneously for achieving a unidirectional radiation and gain enhancement [20]–[23]. Most of these loop-dipole composite antennas can be fabricated by printed broad technique and can achieve unidirectional patterns. But their bandwidth are limited. Although the bandwidth of dual-band loop-dipole composite antenna proposed in [23] can attain about 70%, the geometry of the antenna seems to be complicated and the antenna occupies two layers of the substrate, resulting in fabrication difficulty. Therefore, in order to cover a broader bandwidth and meet certain design requirements such as low-profile, easy fabrication and stable radiation characteristics, it is essential to develop high-performance printed antennas with compact and simple geometry.

As well known, in order to reduce the size of the antennas, some electrically small antenna (ESA) designs based on the popular metamaterials were presented [24]–[26]. And owing to simple, compact structure and good characteristics with negative permeability/permittivity of split-ring resonators (SRRs), it is a kind of widely concerned matermaterial-based resonator [27], [28]. However, the ESA has several disadvanges, such as, narrow band, low radiation efficiency and so on. In this paper, motivated by such tough tasks and inspired by the classic structure of SRRs, a multimode and wideband printed loop composite antenna based on degraded SRRs is proposed. The proposed antenna mainly consists of two coupled rings, which are composed of an outer split ring and one inner closed feed ring. Two coupled rings with big difference in size can be considered as degraded SRRs, which operates at different orthogonal modes, i.e., odd modes of the spilt ring and even modes of closed ring, respectively, such that they works as a compound multimode loop antenna achieving multi-band resonances. Placing a metallic strip close to the inner ring not only induces a new resonant frequency, but also greatly improves the impendence matching among the several resonant frequencies. A coaxial cable with 50-Ohm characteristic impedance is used to excite the inner loop. By virtue of magnetic and electric couplings between two rings, multimode resonances and multi-bands can be generated.

Table 2 compares the performance of the proposed design with other works in previous literature [8], [17], [18], [20], [23]. The proposed antenna not only covers the first split ring mode centered at 816 MHz, but also exhibits a broadband property covering from 2.3 to 4.6 GHz ($|S_{11}| < -10$ dB, 67% fractional bandwidth). With a reduced size as small as 45.7 × 42 mm^2, the fabricated antenna is measured and exhibits a multi-band (including a narrow band at the low frequency and a wide band at the high frequency) impedance matching, average gain of 1 dBi and 3.5 dBi in the low- and high-frequency bands respectively, and more than 80% radiation efficiency. The measured results agree well with simulations and validate the effectiveness of the proposed antenna.

The rest of this paper is structured as follows. In Section II, the configuration of the proposed antenna is given. Evolution of the proposed antenna is analyzed in Section III. The design procedure and working principle of the loop composite antenna is described in detail. The physical mechanism behind the proposed antenna is exploited by the mode analysis and surface current distribution. Section IV presents the experimental prototypes and the radiation performance of the proposed antenna. Finally, the conclusions are drawn in Section V.

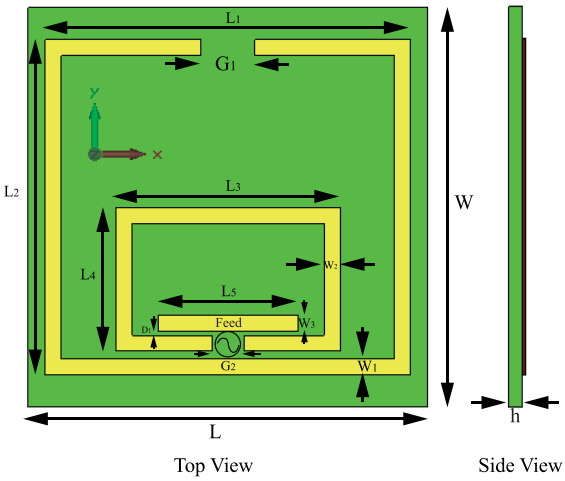

FIGURE 1. Geometry of the proposed antenna.

II. ANTENNA CONFIGURATION AND ANALYSIS

The geometry of the proposed multimode loop antenna is illustrated in Fig. 1. The proposed antenna has a structure printed on a single-layer FR4 dielectric substrate, which has a relative permittivity of 4.4, loss tangent of 0.02 and thickness of 1 mm. The idea of the proposed multimode loop antenna is motivated from the classic metamaterial structure of split ring resonators (SRRs). As shown in Fig. 1, two coupled metallic rings with slits on opposite sides are printed on the top layer of the substrate, where the closed inner ring works as a feeding ring and the outer split ring acts as a coupled loop. Different from the SRRs, there is a significant difference in the sizes of

two split rings. Moreover, in order to expand bandwidth and improve impedance matching, a metallic strip is placed close to the feed gap and inside the inner ring. It is fed by a coaxial cable with 50 Ohm characteristic impedance, where the inner conductor is properly connected to one end of the feed gap and the outer conductor is connected to another end of the feed gap. Numerical simulations and final optimizations are carried out by the CST Microwave Studio (CST-MWS) [29]. The detailed dimensions of the proposed antenna are summarized and listed in Table 1.

TABLE 1. Dimensions for the proposed antenna.

parameter	value(mm)	parameter	value(mm)	parameter	value(mm)
L_1	45.7	L_5	17.5	G_1	6.7
L_2	42	W_1	2	G_2	4
L_3	28	W_2	2	D_1	0.5
L_4	18	W_3	2	h	1

III. EVOLUTION OF THE PROPOSED ANTENNA

As is well known, the traditional loop antenna is directly differential-fed on the ring and its bandwidth is quite small. Inspired by the SRRs, the printed rectangular composite loop antenna composed of a outer split ring and one inner closed ring with big difference in size is herein proposed. In this section, in order to analyze the proposed antenna, the iterative evolution of the proposed antenna is presented. And the design guide and working principle with mode analyse is discussed in detail.

A. DESIGN GUIDES AND MODE ANALYSIS

A set of typical split-ring resonators (SRRs) consists of two metallic concentric and coupled split rings with slits on opposite sides. This specific topology was proposed by Pendry et al. [28] to build up for the negative permeability medium firstly in year 1999. The physical mechanism behind SRRs can be illustrated as follows: when the rings are excited by external time-varying magnetic field along the axial direction, an electromotive force around rings is generated, which in turn induces currents in the rings. The SRRs have been utilized to realize electric small antennas [25]–[28]. As shown in Fig. 2(a), Antenna A based on standard SRRs is fed directly between the slit of the inner ring with the port impedance being set as the input impedance of Antenna A. It is shown that the size of the inner ring and outer split ring is compared

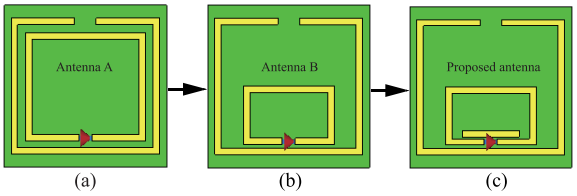

FIGURE 2. Evolution of the proposed antenna. (a) Antenna A based on SRRs. (b) Antenna B based on degraded SRRs. (c) Proposed antenna.

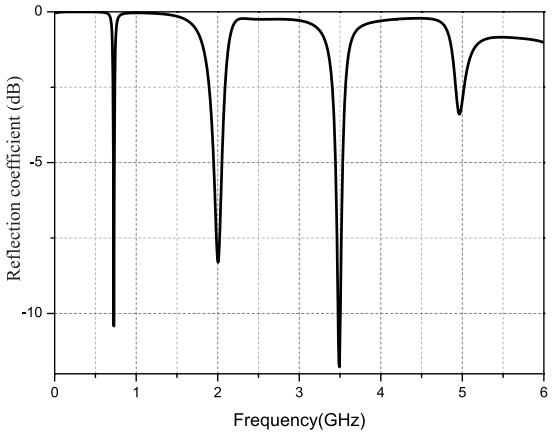

FIGURE 3. Simulated reflection coefficients of the Antenna A.

with each other. As is depicted the simulated reflection coefficients in Fig. 3, although Antenna A can generate multimode and multi-frequency resonances, the resonant frequencies are staggered each other. Therefore, such a kind of antenna can be considered as a narrow-band radiator. Moreover, the real part of input impedance of Antenna A is such too small that the radiation efficiency of Antenna A is very low and the impedance matching with 50 Ohm cable encounters unimaginable difficulties.

In order to get the broadband performance and improve the radiation efficiency of the antenna, the inner ring is shrinked and the outer split ring is enlarged. The loop composite antenna with two rings of large difference in size is formed as depicted in Fig. 2(b) and denoted as Antenna B based on the degraded SRRs. The broadband effect can be obtained by combining the radiating modes of both the inner closed ring and the outer spit ring. In the following, the radiating mechanism and mode analysis about the closed ring and spit ring will be discussed briefly.

From the physical mechanism of resonant mode, one resonant antenna consists of many characteristic modes including non-radiating modes and radiating modes. The typical three different modes, i.e., first, second and third mode, corresponds to various current distributions in Fig. 4. For the first, second and third mode, besides two null ends of the aperture, there are zero, one, two null nodes such that one-direction, two reverse and three reverse current distributions on the aperture can be achieved respectively. Herein, the split ring can be consider as a bent dipole, having two open ends and the closed ring can be considered as having one combining end. The above feature of the split ring and closed ring will determine their difference of the non-radiating mode and radiating mode.

In Fig. 5(a), the split ring with the same size as the outer ring of Antenna B is simulated individually. It can be seen that, although there is some impedance mismatching between the feeding port and the split ring, the resonant frequencies and modes can be seen clearly in Fig. 5(b). From the theory of the antenna resonance, the fundamental resonant mode is

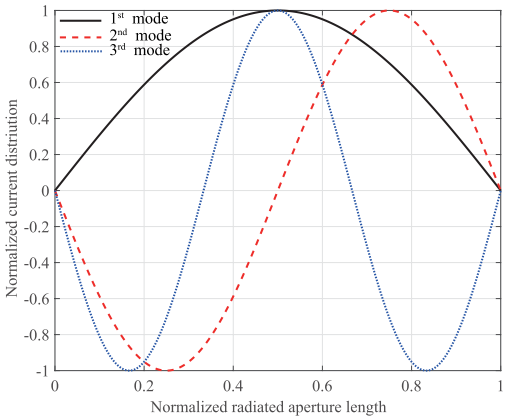

FIGURE 4. Current distribution of first, second, and third mode on the line aperture.

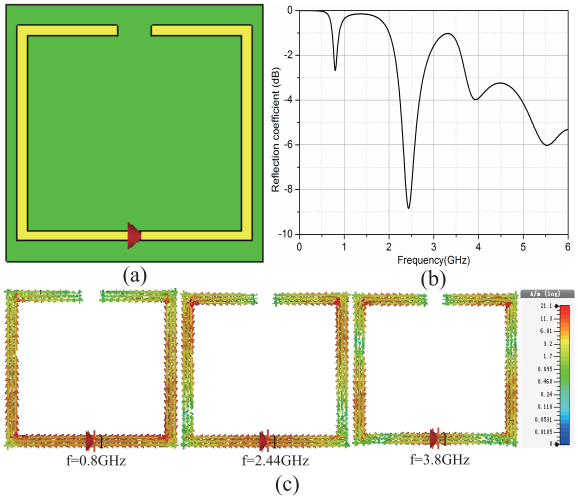

FIGURE 5. Analysis of the split ring. (a) configuration of the split ring, (b) reflection coefficients, (c) current distribution at 0.8, 2.44 and 3.8 GHz, respectively.

the half-wavelength resonant mode, which is in accordance to the first mode in Fig. 4. The rough estimation of split ring can be approximately calculated with half effective wavelength,

$$f_L \approx \frac{c}{2\sqrt{\varepsilon_{eff}}(2L_1 + 2L_2 - G_1)} \tag{1}$$

where $\varepsilon_{eff} \approx (\varepsilon_r + 1)/2$ and ε_r is the dielectric constant of the substrate. $2L_1 + 2L_2 - G_1$ is equal to the perimeter of the outer ring and c denotes the light speed in free space. This exact length will be optimized by full-wave optimization for the whole antenna structure. In our design, its resonance frequency is chosen as about 0.8 GHz in Fig. 5(b), which is the first resonant mode of the split ring. As depicted in Fig. 5(c), the current distribution flows along one direction and no null nodes exist, such that fundamental mode (first mode) can be obtained. The second mode at about 1.6 GHz is non-radiating mode, so there is no resonance at about 1.6 GHz in Fig. 5(b). Moreover, as shown in Fig. 5(b), the third mode at about 2.4 GHz can be obtained such that two null nodes on the current distribution can be formed. The fifth mode at about 3.8 GHz can be got, where there are four null nodes on the current distribution in Fig. 5(c). And so on, for the split ring, the even modes are the non-radiating modes and the odd modes belongs to the radiating mode.

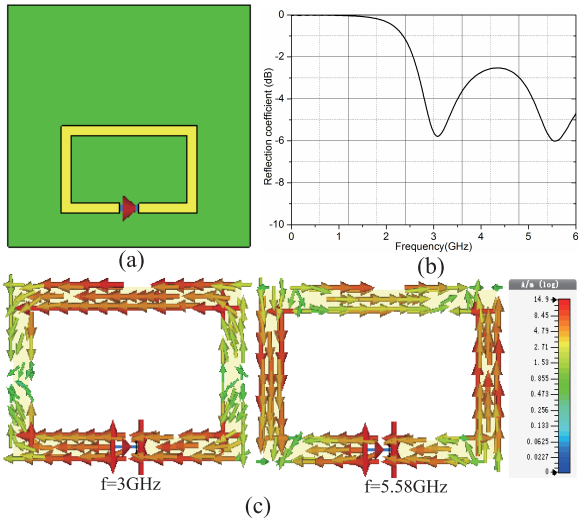

FIGURE 6. Analysis of closed ring. (a) Configuration of the closed ring. (b) Reflection coefficients. (c) Current distribution at 3 and 5.58 GHz, respectively.

In Fig. 6(a), the closed inner ring is also simulated and analyzed independently. Different from the split ring, the two end nodes in the split ring are merged into one node in the closed ring. As for the closed ring, including one merged null node, there are one, two, three null nodes on the current distribution for first, second and third mode, respectively. Consequently, as shown in Fig. 6, the first resonant frequency at about 3 GHz is a radiating mode. And according to the current distribution in Fig. 6, the first resonant frequency belong to the second mode, i.e., one-wavelength loop mode. So the roughly estimated length of the inner ring $(2L_3 + 2L_4)$ can be approximately obtained by,

$$f_M \approx \frac{c}{\sqrt{\varepsilon_{eff}}(2L_3 + 2L_4)}. \tag{2}$$

And the second resonant frequency at about 5.58 GHz, which has four null nodes on the current distribution, is the fourth mode of the closed ring. Therefore, as for the closed ring, the even modes are the radiating modes and the odd modes are the non-radiating modes, which is just the opposite case of the split ring. In conclusion, from the characteristic mode analysis, the radiating modes of the split ring and closed ring are orthogonal to each other.

By virtue of the mode orthogonality theory above, the split ring and closed ring can be combined together and the mutual coupling between the two radiators can be easily controlled. And being combined the two resonant rings in Fig. 5 and Fig. 6 together, the Antenna B can be formed. In the configuration of Antenna B, the edge along the feed of the inner rings are close to the edge at the bottom of the outer

ring, so the magnetic and electric couplings between the inner and outer rings are formed. The capacitive coupling is formed between the edge of the inner ring to the edge at the bottom of the outer ring and the inductive coupling is generated between the two rings. As analysed above, the resonant frequencies at odd radiating mode of the outer spit ring are about 0.8 GHz, 2.44 GHz, and 3.8 GHZ and the resonant frequencies at even radiating modes of the inner closed ring are 3 GHz, 5.58 GHz. By combined the radiating modes of two rings properly, the effect of broadband at high frequencies band composed of multi-band resonances is achieved. As shown in Fig. 7(a), By feeding the inner ring and with electric and magnetic couplings to outer split ring, Antenna B not only covers the first mode of split ring at about 816 MHz, but also exhibits a quite broadband property ranging from 2.4 to 3.8 GHz.

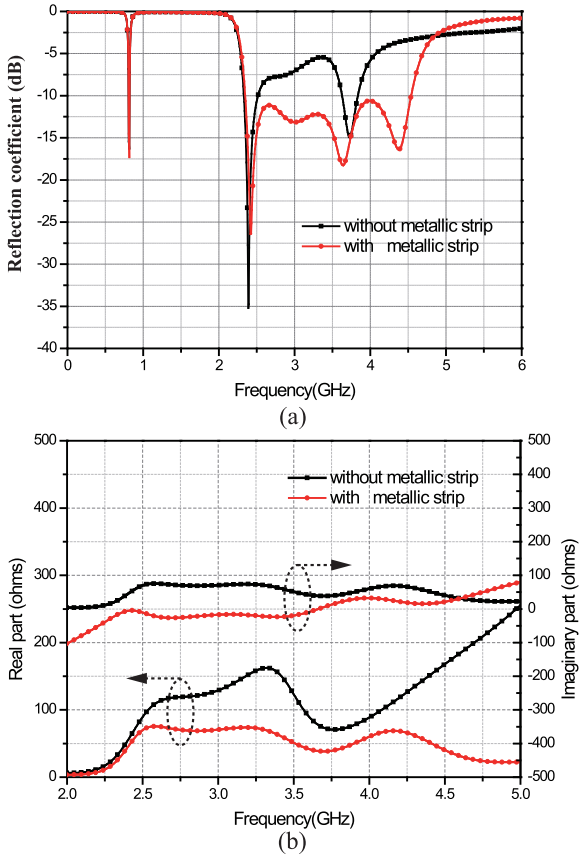

FIGURE 7. (a) Simulated reflection coefficients and (b) input impedances of the proposed antenna with and without the parasitic strip.

However, a observation can be drawn that the impedance matching of Antenna B is unsatisfactory at the high frequency band, in which the reflection coefficient at most of the frequencies is larger than -10 dB. To improve the impedance matching at the high frequency band, a parasitic strip is added adjacent to the feed gap of the inner ring and the final proposed multimode loop antenna based on degraded SRRs is then constructed. Here the parasitic strip not only supply the capacitive loading for impedance matching but also act as a radiator dipole coupling by the inner ring. In the following, the proposed antenna will be analyzed and discussed in detail.

B. EFFECT OF PARASITIC STRIP

To illustrate how the parasitic strip affects the antenna performance, some simulation and discussion would be proceeded in the following.

1) ANALYSIS OF PARASITIC STRIP

As discussed above, the main difference between Antenna B and the proposed antenna is the parasitic strip. As shown in Fig. 7(a), the reflection coefficients of Antenna B and proposed antenna are compared with each other. It is able to be observed that there are three resonant frequencies for Antenna B while four different resonant frequencies for the proposed antenna. The fourth resonant frequencies can be determined by the parasitic strip, which act as a radiator dipole coupling by the inner ring. Therefore the length of the parasitic strip (L_5) can be approximately calculated by

$$f_H \approx \frac{c}{2\sqrt{\varepsilon_{eff}}(L_5)}. \tag{3}$$

Moreover, the impedance matching of the proposed antenna is much better than Antenna B at the high frequencies. The impedance bandwidth for $|S_{11}| < -10$ dB of the proposed antenna at high frequency band covers wide bandwidth from 2.3 to 4.6 GHz, which is much larger than Antenna B without the parasitic strip. Therefore, after the parasitic strip beside the feed gap is added, both the impedance matching and the bandwidth are improved significantly at high frequency band. To explain the working principle of the parasitic strip from the input impedance, the simulated input impedances of the antennas with and without the parasitic strip are shown in Fig. 7(b). As indicated in Fig. 7(b), a better input impedance can be obtained by using the parasitic strip, by which the coaxial cable with 50 Ohms characteristic impedance can be matched more easily. The real part of input impedance in the proposed antenna is closer to 50 ohms, and the imaginary part is closer to 0 Ohms. The physical mechanism behind of the performance can be illustrated as follows: 1) the parasitic strip can act as impedance matching and transformation. By adjusting the distance between the parasitic strip and the feed gap the capacitive impedance can be changed, whereas by adjusting the length of the parasitic strip the inductive impedance can be shifted. 2) the parasitic strip itself also works as a dipole radiator and generates a new resonant frequency at high frequency band. By virtue of these two kinds of physical mechanism, the impedance matching is greatly improved among the several resonant frequencies and the bandwidth can be enhanced greatly.

2) EFFECTS OF PARASITIC STRIP

In order to further investigate the effect of the parasitic strip and validate the physical mechanism, the parametric sweep and analysis of the parasitic strip length (L_5) and position (D_1) are performed in detail in this subsection.

The performance on the reflection coefficient with different lengths (L_5) and positions (D_1) of the parasitic strip is shown in Fig. 8. It is shown in Fig. 8(a), the upper

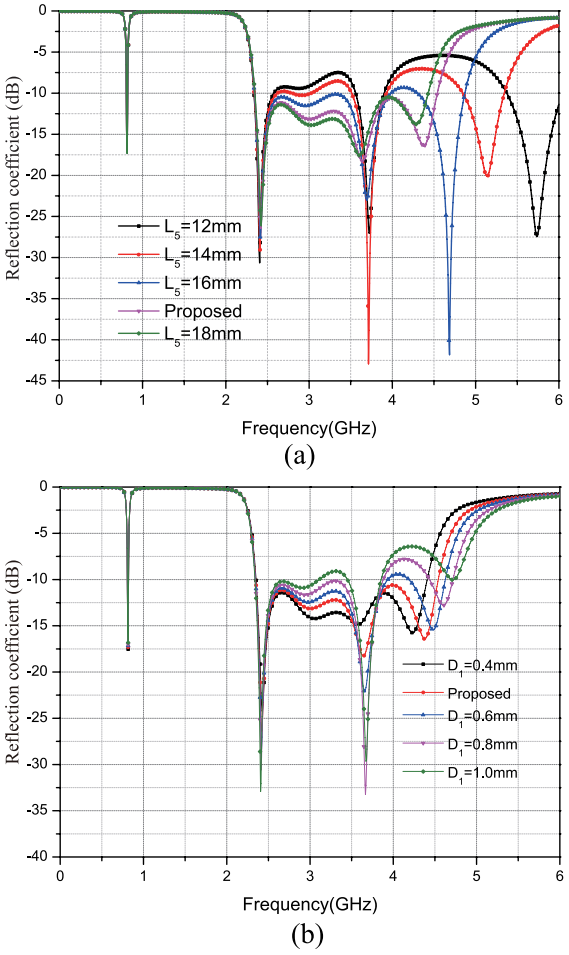

FIGURE 8. The effects of different (a) length and (b) position of the parasitic strip on the reflection coefficient.

resonant frequency at high frequency band is mainly determined by the parasitic strip. When the length (L_5) of the parasitic strip increases, the upper resonant frequency shifts towards lower frequency and the impedance matching at the whole high band has been improved as well, whereas the other frequencies are almost unaffected with L_5. Also, from Fig. 8(b), it can be seen, as the distance between the inner split rectangular loop and the parasitic strip D_1 decreases (i.e., D_1 from 1 mm to 0.4 mm), the impedance matching at the upper band is significantly improved. Therefore, the upper band-edge selectivity can be determined by L_5 and D_1 independently. Overall in the proposed loop antenna, one can see that $L_5 = 17.5$ mm, $D_1 = 0.5$ mm are the best choice for fully considering both the impedance matching and the bandwidth at the whole bands. Thus the resonant frequency and the impedance matching of high band could be adjusted and optimized individually by the length and the relative position of the parasitic strip, respectively.

C. SURFACE CURRENT DISTRIBUTION ANALYSIS

To better understand the behavior of the proposed antenna, the corresponding surface current distribution on the radiator and the stubs are illustrated. As described in Sections A and B, the proposed antenna is more analogous to composite double loop antenna loaded a parasitic strip, which have multiple operational modes including split ring mode by magneto-electric coupling, closed loop mode and electric coupling dipole mode. Based on the qualitatively initial analyses about reflection coefficients above, the surface current distributions at four different resonant frequencies, 0.816 GHz, 2.42 GHz, 3.65 GHz and 4.38 GHz, are studied and depicted in Fig. 9(a), (b), (c) and (d), respectively.

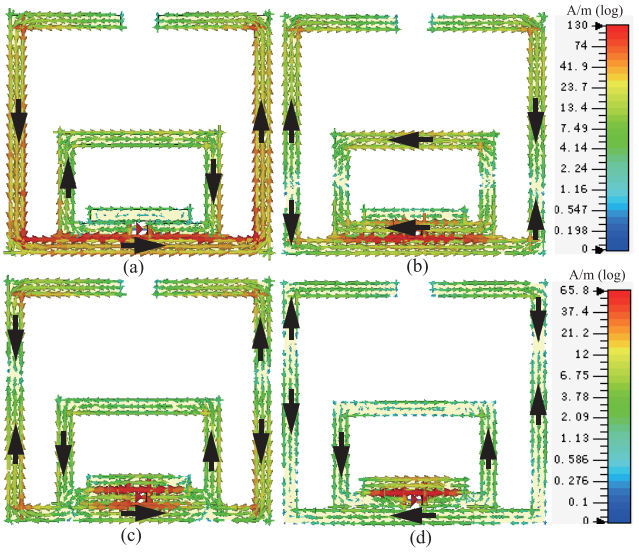

FIGURE 9. Simulated current distribution of proposed antenna at different frequencies. (a) 0.816 GHz. (b) 2.42 GHz. (c) 3.65 GHz. (d) 4.38 GHz.

As shown in Fig. 9(a), at 0.816 GHz, the perimeter of the outer ring is about half effective wavelength. And the current distribution is mainly concentrated on the edge of the outer ring while the current distribution on the inner ring can be negligible, where the current flowing on both of the rings are just in one direction and no null nodes exist. At 0.816 GHz, the outer split ring operates as the first radiating mode, whereas, the inner closed ring works as the first non-radiating mode. Therefore the working radiating mode of the split ring are not affected by the non-radiating mode of closed ring.

In Fig. 9(b), at 2.42 GHz, one can see that the current distribution is mainly concentrated on the edges of both of the rings. However, the current distribution shown in Fig. 9(b) indicates that there are two null points at the left and right edges along the y-axis on both of the rings. And the outer split ring operates at the third radiating mode and inner closed ring works at the second radiating mode. From the analysis in Section III, the main radiator is the outer split ring, which is resonant at the $3f_L$ and the inner closed ring acts as a feeding loop. The odd and even working modes are mutually orthogonal and the working frequencies for two rings are different such that the mutual radiating interference

is quite little. The coupling between the inner and outer rings consists of electric coupling and magnetic coupling. Specifically, the electric coupling, also called the capacitive coupling, is introduced between the edge fed in the inner ring and the edge at the bottom of the outer ring. One can see that the current distributions on the two edges are the strongest. On the other hand, the magnetic coupling, also called the inductive coupling, is caused by the shared magnetic field between the rings. Therefore, the proposed antenna mainly operates at the third mode of split ring by magnetic-electric coupling.

At 3.65 GHz, as depicted in Fig. 9(c), the surface current also distributed on both of the rings. Different from 2.42 GHz, there are four null nodes on the outer split ring such at it operates at the fifth radiating mode. And in the same way the inner ring working at the second radiating mode act as an excitation for the outer split ring. The radiating interference between the two modes is a little more than case at 2.42 GHz. And the resonant frequency, i.e., 3.65 GHz is a little smaller than $5f_L$. From the surface current distribution, it is proved that the proposed antenna also mainly operates the fifth mode of the split ring feeding by the second mode of the inner closed ring.

At 4.38 GHz, it can be seen from Fig. 9(d), the current distribution is mainly concentrated on the short parasitic strip. And the proposed antenna resonates as a half-wavelength dipole and is fed by electric coupling between the feed strip and the parasitic strip.

Based on the analyses, the current distribution illustrates the physical mechanism behind the proposed antenna well and demonstrates that the proposed antenna utilizes both the electric and magnetic couplings and operates in multimodes at the resonate frequencies. From the simulation results above, it can be summarized that the broadband at the high frequencies is composed of the odd radiating modes (third and fifth mode) of the outer split ring, the even radiating mode (second mode) of inner closed ring and the half-wavelength dipole mode of the parasitic strip. And the mutual interference among different radiating modes is so small that all the resonant frequencies can be almost individually determined and optimized by various radiators. The measured results of the designed antenna are discussed in the next section.

IV. PERFORMANCE AND DISCUSSION

A. REFLECTION COEFFICIENTS

In this section, to experimentally verify the effectiveness of the proposed design, a prototype of the proposed antenna is fabricated according to the optimized dimensions summarized in Table 1. Photographs of the fabricated antenna are shown in Fig. 10. A 50 ohm coaxial cable with a SMA connector is used to feed the antenna for the measurement. The inner conductor of coaxial cable is connected to one arm of the inner rectangular loop, whereas the outer conductor of the cable is soldered to the other arm. The reflection coefficients

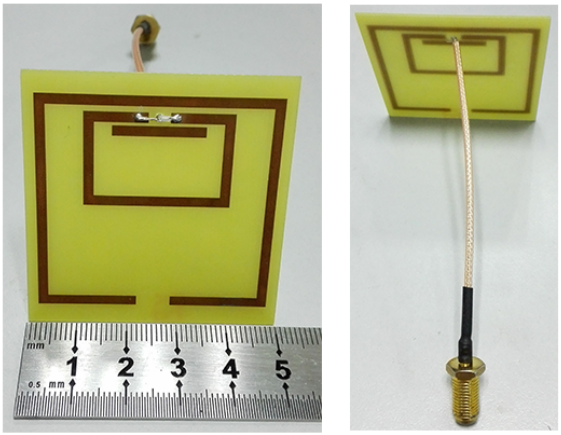

FIGURE 10. Photographs of the fabricated antenna. (a) Front view. (b) Back view.

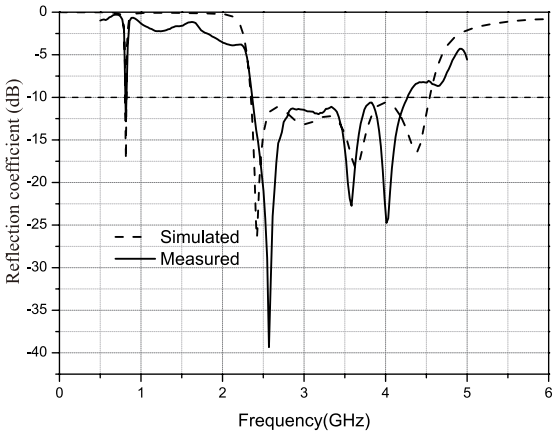

FIGURE 11. Comparison of the measured and simulated reflection coefficients of the proposed antenna.

of the proposed antenna are measured by the Agilent E8363B VNA. The measured and simulated reflection coefficients are depicted in Fig. 11. Matching with $|S_{11}| < -10$ dB is achieved across the bandwidth of interest. As indicated in Fig. 11, good agreement is achieved between the simulated and measured results. Meanwhile, as expected, an excellent impedance matching and wide operating band are observed. According to the measured result, the percentage bandwidth (with the criteria of $|S_{11}| < -10$ dB) of the fabricated antenna is approximately 60.6% ranging from 2.3 to 4.3 GHz. Although there are some differences between the simulated and measured results, especially in high frequency bands. The slight differences, which are most likely due to variations in permittivity, thickness of substrate, the coaxial feeding cable and the uncertain factors of the fabricating and manufacturing, are acceptable in general. Based on the results in Figs. 7, 8 and 11, it has been numerically and experimentally proved that the broadband, good impedance matching and multimode operating characteristics of antenna are depended on the jointly effect of the double loops and the additional parasitic strip.

B. RADIATION PATTERNS, EFFICIENCY, AND GAIN

The antenna is measured in an anechoic chamber. The normalized radiation patterns of the simulated and measured at the two main radiation planes (E-Plane (xoz-plane) and H-Plane (yoz-plane)) at different frequencies 0.816, 2.42, 3.65 and 4.38 GHz are presented in Fig. 12. It can be observed that the simulated and measured patterns agree well with each other. The radiation patterns of the proposed antenna exhibit omnidirectional and quasi-omnidirectional radiation characteristics at 0.816 GHz and 2.42 GHz, respectively. All the H-plane patterns exhibit quasi-omnidirectional properties and the E-plane radiations have different quasi-symmetrical dipole-like patterns with respect to different fed wavelengths. However, with the increase of the operating frequency, the designed antenna exhibits some unidirectional radiation characteristics in H-plane at 3.65 GHz and 4.38 GHz. In E-plane, quasi-symmetrical dipole-like patterns can be also obtained. The unidirectional radiation patterns at 3.65 and 4.38 GHz probably cased by co-dominated by the high-order split ring mode and loaded-dipole mode feeding by inner close ring. The loop-dipole radiation patterns can be obtained, which can be also illustrated from the surface current distributions in Fig. 9. Moreover, the measured cross-polarization patterns within the main beam of E- and H-planes are also depicted in Fig. 12. The cross-polarization levels in both E- and H-planes are generally below −18 dB.

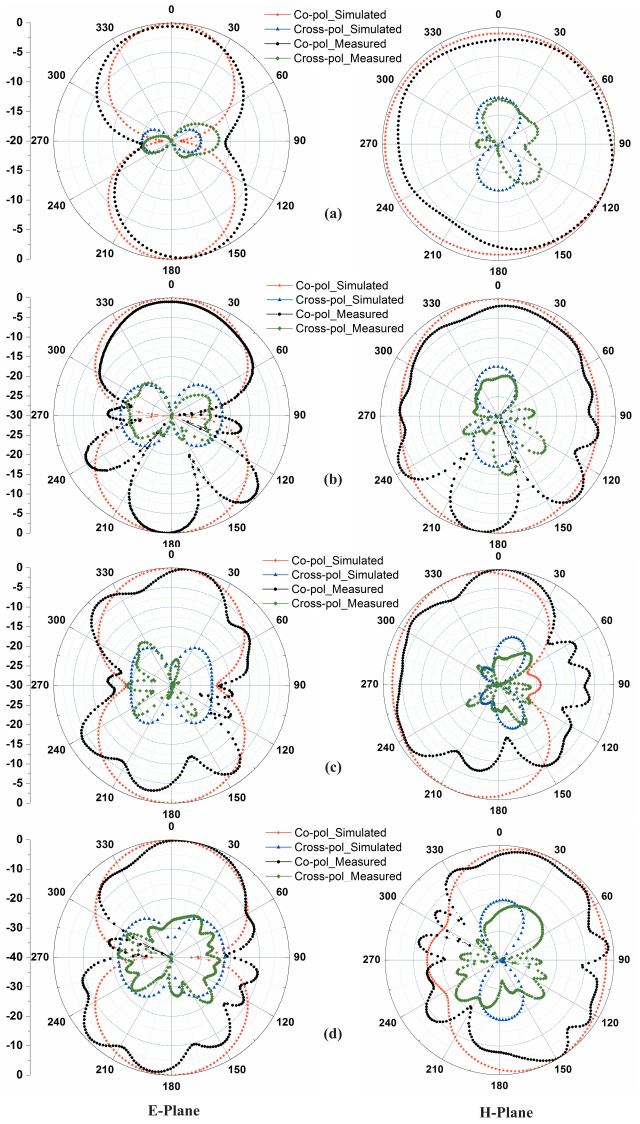

FIGURE 12. Measured and simulated radiation patterns of the proposed antenna at (a) 0.816 GHz, (b) 2.42 GHz, (c) 3.65 GHz, and (d) 4.38 GHz.

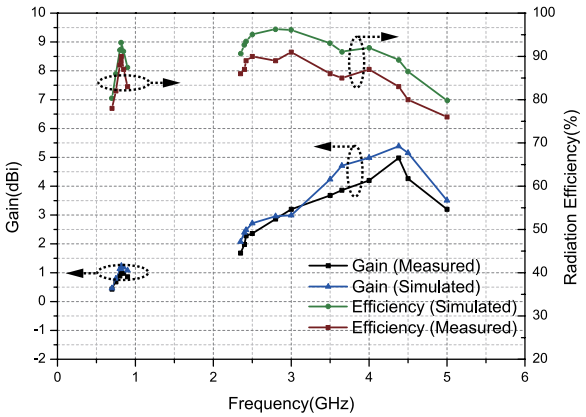

FIGURE 13. Measured and simulated antenna gain and radiation efficiency of the proposed antenna.

The simulated and measured gains and efficiencies are plotted in Fig. 13. Within the lower resonant frequency point (0.816 GHz), the measured peak gain is about 1.2 dBi, while in the higher frequency band (2.3-5 GHz), the measured average gain is about 3.5 dBi (1.8-5.1 dBi). Generally speaking, with an increase of the resonant frequency, the gain is also improved. The maximum gain (i.e., 5.1 dBi) can be attained at 4.38 GHz, just as analysis that the proposed antenna exhibits unidirectional characteristics at high frequency band. The simulated and measured gains agree quite well with each other with maximum error of about 0.9 dB. Also the measured average efficiency is 82% in the low frequency band and 85% in the high frequency band. High efficiency in the low frequency band confirms that the proposed antenna doesn't work at standard ESA mode based on SRRs, but a new-style mode based on degraded SRRs. The efficiency is relatively stable across the higher operating frequency band (2.3-4.6 GHz). However, the radiation efficiency drops quickly when the frequency is higher than 4.6 GHz. It is mainly due to the larger impedance mismatching and feed cable loss. The simulated results agree well with the measured efficiency. Although slight difference could be attributed to the uncertainty regarding the material, the feed coaxial cable and the fabrication tolerances at these frequencies. Table 2 is prepared to compare the proposed antenna with other reported loop antennas in terms of bandwidth, sizes, antenna geometry and radiator type.

TABLE 2. Comparison between the proposed antenna with other designs.

References	Fractional bandwidth (VSWR $\leq$ 2, GHz)	Overall dimension (mm^3)	Antenna configuration	Radiator type
[8]	10.8% (1.414-1.576)	$130 \times 110 \times 19.8$	Three dimensional	Loop and disk-loaded monopole
[17]	49% (0.7-1.15)	$120 \times 120 \times 0.8$	Two-layer printed antenna	Loop-dipole composite antenna
[18]	40.7% (2.29-3.46)	$60 \times 50 \times 0.5$	Uni-planar printed antenna	Loop antenna
[20]	7.4% (2.35-2.53)	$51 \times 41 \times 1.6$	Uni-planar printed antenna	Loop-dipole composite antenna
[23]	71.1%,32.9% (1.54-3.24,4.88-6.8)	$70 \times 60 \times 0.508$	Two-layer printed antenna	Magneto-electric dipole
This work	67% 2.3-4.6	$50 \times 50 \times 1$	Uni-planar printed antenna	Loop-meta composite antenna

V. CONCLUSION

A compact, multimode and wideband compound loop antenna with degraded SRRs and a parasitic stirp was presented. By magnetic and electric couplings among the two rings and the parasitic strip, three different types of resonant modes, i.e., the odd mode of the spilt ring, the even mode of the closed ring and the dipole mode of the parasitic strip, can be achieved. By both simulations and experiments, it has been shown that the proposed loop antenna covers two operating bands: a narrow band of the first split ring mode centered at 816 MHz and a broadband with 67% factional bandwidth from 2.3 to 4.6 GHz, which is composed of three different resonant modes: third and fifth mode of the split ring, second mode of the inner closed ring, half-wavelength dipole mode. Especially, by introducing the parasitic strip adjacent to the feed gap, the impedance matching and bandwidth at the high frequency band can be improved greatly without any effect on the low frequency band. It was also shown that the average gain of 1 dBi and 3.5 dBi in the two bands, average efficiency of 82% at the low frequency band and 85% at the high frequency band, stable omnidirectional E-plane radiation pattern and some H-plane unidirectional characteristics at the high frequency band with low cross polarization are obtained. The proposed antenna occupies only an area of 45.7×42 mm^2, which is, to the best of our knowledge, the smallest loop-type antenna with similar bandwidth and radiation performance [16]–[23]. The good characteristics of wideband, uniplanar and simple printed structure, high efficiency and nice radiation patterns make the proposed loop antenna capable of being used in a wide range of wireless applications.

REFERENCES

[1] S. A. Rezaeieh, A. Zamani, K. Bialkowski, and A. Abbosh, "Foam embedded wideband antenna array for early congestive heart failure detection with tests using artificial phantom with animal organs," *IEEE Trans. Antennas Propag.*, vol. 63, no. 11, pp. 5138–5143, Nov. 2015.

[2] S. Shadrokh, Y. Q. Yu, F. Jolani, and Z. Chen, "Ultra-compact end-loaded planar dipole antenna for ultra-wideband radar and communication applications," *Electron. Lett.*, vol. 50, no. 21, pp. 1495–1496, Oct. 2014.

[3] O. T.-C. Chen and C.-Y. Tsai, "CPW-fed wideband printed dipole antenna for digital TV applications," *IEEE Trans. Antennas Propag.*, vol. 59, no. 12, pp. 4826–4830, Dec. 2011.

[4] O. Caytan *et al.*, "Half-mode substrate-integrated-waveguide cavity-backed slot antenna on cork substrate," *IEEE Antennas Wireless Propag. Lett.*, vol. 15, pp. 162–165, May 2015.

[5] L. Ge and K. M. Luk, "A magneto-electric dipole antenna with low-profile and simple structure," *IEEE Antennas Wireless Propag. Lett.*, vol. 12, pp. 140–142, 2013.

[6] Q. Wu, R. Jin, and J. Geng, "A single-layer ultrawideband microstrip antenna," *IEEE Trans. Antennas Propag.*, vol. 58, no. 1, pp. 211–214, Jan. 2010.

[7] K.-M. Luk and H. Wong, "A new wideband unidirectional antenna element," *Microw. Opt. Technol. Lett.*, vol. 1, no. 1, pp. 35–44, 2006.

[8] W.-T. Hsieh and J.-F. Kiang, "Small broadband antenna composed of dual-meander folded loop and disk-loaded monopole," *IEEE Trans. Antennas Propag.*, vol. 59, no. 5, pp. 1716–1720, May 2011.

[9] S. I. Latif, L. Shafai, and S. K. Sharma, "Bandwidth enhancement and size reduction of microstrip slot antennas," *IEEE Trans. Antennas Propag.*, vol. 53, no. 3, pp. 994–1003, Mar. 2005.

[10] S.-W. Qu, J.-L. Li, Q. Xue, and C.-H. Chan, "Wideband periodic endfire antenna with bowtie dipoles," *IEEE Antennas Wireless Propag. Lett.*, vol. 7, pp. 314–317, 2008.

[11] C. F. Tseng and C. L. Huang, "A wideband cross monopole antenna," *IEEE Trans. Antennas Propag.*, vol. 57, no. 8, pp. 2464–2468, Aug. 2009.

[12] T.-G. Ma and S.-K. Jeng, "A printed dipole antenna with tapered slot feed for ultrawide-band applications," *IEEE Trans. Antennas Propag.*, vol. 53, no. 11, pp. 3833–3836, Nov. 2005.

[13] K. Xu, Z. Zhu, H. Li, J. Huangfu, C. Li, and L. Ran, "A printed single-layer UWB monopole antenna with extended ground plane stubs," *IEEE Antennas Wireless Propag. Lett.*, vol. 12, pp. 237–240, 2013.

[14] A. P. Gorbachev, O. O. Kibirev, and V. S. Churkin, "A modified broad-band planar quasi-yagi antenna," in *Proc. 10th Int. Sci.-Technol. Conf. Actual Problems Electron. Instrum. Eng. (APEIE)*, Jun. 2010, pp. 46–48.

[15] R. Li, G. DeJean, M. Tentzeris, J. Laskar, V. Fusco, and R. Cahill, "Unidirectional printed loop antenna," in *Proc. 6th Int. Symp. Antennas, Propag. EM Theory*, 2003, pp. 104–107.

[16] J. Wu, Z. Zhao, Z. Nie, and Q. H. Liu, "A printed unidirectional antenna with improved upper band-edge selectivity using a parasitic loop," *IEEE Trans. Antennas Propag.*, vol. 63, no. 4, pp. 1832–1837, Apr. 2015.

[17] S. A. Rezaeieh and A. Abbosh, "Compact planar loop–dipole composite antenna with director for bandwidth enhancement and back radiation suppression," *IEEE Trans. Antennas Propag.*, vol. 64, no. 8, pp. 3723–3728, Aug. 2016.

[18] J. Wu, Z. Zhao, Z. Nie, and Q. H. Liu, "A broadband unidirectional antenna based on closely spaced loading method," *IEEE Trans. Antennas Propag.*, vol. 61, no. 1, pp. 109–116, Jan. 2013.

[19] S. A. Rezaeieh, A. Zamani, K. S. Bialkowski, and A. M. Abbosh, "Unidirectional slot-loaded loop antenna with wideband performance and compact size for congestive heart failure detection," *IEEE Trans. Antennas Propag.*, vol. 63, no. 10, pp. 4557–4562, Oct. 2015.

[20] H. W. Lai and H. Wong, "Substrate integrated magneto-electric dipole antenna for 5G Wi-Fi," *IEEE Trans. Antennas Propag.*, vol. 63, no. 2, pp. 870–874, Feb. 2015.

[21] H. W. Lai, K. K. So, H. Wong, C. H. Chan, and K. M. Luk, "Magnetoelectric dipole antennas with dual open-ended slots excitation," *IEEE Trans. Antennas Propag.*, vol. 64, no. 8, pp. 3338–3346, Aug. 2016.

[22] H. Wang, S.-F. Liu, L. Chen, W.-T. Li, and X.-W. Shi, "Gain enhancement for broadband vertical planar printed antenna with H-shaped resonator structures," *IEEE Trans. Antennas Propag.*, vol. 62, no. 8, pp. 4411–4415, Aug. 2014.
[23] W.-J. Lu, G.-M. Liu, K. F. Tong, and H.-B. Zhu, "Dual-band loop-dipole composite unidirectional antenna for broadband wireless communications," *IEEE Trans. Antennas Propag.*, vol. 62, no. 5, pp. 2860–2866, May 2014.
[24] J. B. Pendry, A. J. Holden, D. J. Robbins, and W. J. Stewart, "Magnetism from conductors and enhanced nonlinear phenomena," *IEEE Trans. Microw. Theory Techn.*, vol. 47, no. 11, pp. 2075–2084, Nov. 1999.
[25] L. Wang, M. Q. Yuan, and Q. H. Liu, "A dual-band printed electrically small antenna covered by two capacitive split-ring resonators," *IEEE Antennas Wireless Propag. Lett.*, vol. 10, pp. 824–826, 2011.
[26] L. Peng, P. Chen, A. Wu, and G. Wang, "Efficient radiation by electrically small antennas made of coupled split-ring resonators," *Sci. Rep.*, vol. 6, Sep. 2016, Art. no. 33501.
[27] A. Erentok and R. W. Ziolkowski, "Metamaterial-inspired efficient electrically small antennas," *IEEE Trans. Antennas Propag.*, vol. 56, no. 3, pp. 691–707, Mar. 2008.
[28] R. W. Ziolkowski and A. Erentok, "Metamaterial-based efficient electrically small antennas," *IEEE Trans. Antennas Propag.*, vol. 54, no. 7, pp. 2113–2130, Jul. 2006.
[29] M. Jin, *Antenna Simulation and Engineering Design With CST* , Beijing, China: House of Electronics Industry, 2014.

KUIWEN XU received the B.E. degree from Hangzhou Dianzi University, China, in 2009, and the Ph.D. degree from Zhejiang University, Hangzhou, China, in 2014.

He was a Visiting Ph.D. Student with the National University of Singapore from 2012 to 2013. From 2014 to 2015, he was with Huawei Technologies Company Ltd. He is currently an Associate Professor with Hangzhou Dianzi University. His research interests include antenna design, microwave measurement, and electromagnetic inverse problems.

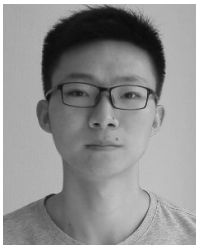

FEI LIU received the B.S. degree in communication engineering from West Anhui University, Lu'an, China. He is currently pursuing the M.S. degree in electromagnetic field and microwave technology with Hangzhou Dianzi University, Hangzhou, China. His research interests include multiband mobile antenna, printed broadband antenna, and electrically small antenna.

LIANG PENG received the B.S. and Ph.D. degrees from Zhejiang University, Hangzhou, China, in 2003 and 2008, respectively. He held a postdoctoral position with the Technical University of Denmark from 2009 to 2011. In 2011, he joined Hangzhou Dianzi University and became a Research Associate in 2012. His research interests include electromagnetic theory, artificial metamaterials, new concept antennas, optical plasmonics, and topological photonics.

WEN-SHENG ZHAO (S'09–M'14) received the B.Eng. degree in electronic science and technology from the Harbin Institute of Technology, Harbin, China, in 2008, and the Ph.D. degree in electronic science and technology from Zhejiang University, Hangzhou, China, in 2013.

He was a Visiting Ph.D. Student with the National University of Singapore from 2010 to 2013. Since 2013, he has been a Faculty Member with Hangzhou Dianzi University, Hangzhou, China, where he is currently an Associate Professor. His research interests include interconnect design and simulation, carbon nanoelectronics, electromagnetic compatibility, and multiphysics simulation.

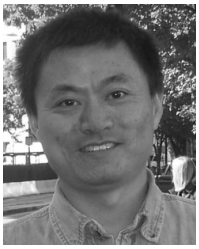

LIXIN RAN received the B.S., M.S., and Ph.D. degrees from Zhejiang University, Hangzhou, China, in 1991, 1994, and 1997, respectively. In 1997, he became an Assistant Professor, in 1999, an Associate Professor, and in 2004, a Full Professor with the Department of Information and Electronics Engineering, Zhejiang University, Hangzhou, China. In 2005, 2009, and 2012, he visited the Massachusetts Institute of Technology, Cambridge, MA, USA, as a Visiting Scientist. He is currently the Director of the Laboratory of Applied Research on Electromagnetics with Zhejiang University. He has co-authored more than 120 research papers published in peer-reviewed journals. He holds more than 30 patents. His research interests include new concept antennas, radio-aware sensing and imaging, RF, microwave and terahertz systems, and artificial active media.

GAOFENG WANG (S'93–M'95–SM'01) received the Ph.D. degree in electrical engineering from the University of Wisconsin–Milwaukee, Milwaukee, WI, USA, in 1993, and the Ph.D. degree in scientific computing from Stanford University, Stanford, CA, USA, in 2001.

He was a Scientist with Tanner Research Inc., Pasadena, CA, USA, from 1993 to 1996. He was a Principal Researcher and Development Engineer with Synopsys Inc., Mountain View, CA, USA, from 1996 to 2001. In 1999, he served as a Consultant with Bell Laboratories, Murray Hill, NJ, USA. He was the Chief Technology Officer (CTO) of Intpax, Inc., San Jose, CA, USA, from 2001 to 2003. He was the CTO of Siargo Inc., Santo Clara, CA, USA, from 2004 to 2010. He was a Professor and the Head of the CJ Huang Information Technology Research Institute with Wuhan University, Wuhan, China, from 2004 to 2013. He was the Chief Scientist with Lorentz Solution, Inc., Santa Clara, CA, USA, from 2010 to 2013. He is currently a Distinguished Professor with Hangzhou Dianzi University, Hangzhou, China. He has authored more than 160 journal articles and holds 22 patents. His current research interests include integrated circuit and microelectromechanical system design and simulation, computational electromagnetics, electronic design automation, and wavelet applications in engineering.